Mon. Not. R. Astron. Soc. **000**, 000–000 (0000) Printed 2 October 1997

Interacting OB star binaries: LZ Cep, SZ Cam and IU Aur

T.J. Harries,[1,2] R.W. Hilditch,[1] and G. Hill[3]

[1] *School of Physics & Astronomy, University of St. Andrews, North Haugh, St. Andrews, Fife KY16 9SS, Scotland.*
[2] *Now at: Mullard Space Science Laboratory, University College London, Holmbury St. Mary, Dorking, Surrey RH5 6NT, UK.*
[3] *18A Stratford Street, Auckland 1, New Zealand.*

Dates to be inserted

ABSTRACT

New spectroscopic observations of three O+O binary stars (LZ Cep, SZ Cam and IU Aur), obtained over a number of years at the Dominion Astrophysical Observatory, are analyzed using state-of-the-art cross-correlation techniques to produce radial velocity curves. These results are combined with new (LZ Cep) and published (SZ Cam and IU Aur) photometry to yield masses, temperatures, radii and luminosities.

We find that LZ Cep is a semi-detached system, in agreement with the results of Howarth et al. (1991), with the secondary star filling its Roche lobe. We find a distance modulus of 9.6 ± 0.2, which is slightly smaller than the distance modulus to Cep OB2 (=9.9, Garmany & Stencel 1992).The reddening of LZ Cep is also at the lower end of the cluster range, suggesting that the binary is located on the cluster's near side.

SZ Cam is a triple system, and we are able to measure the radial velocities of the three components that are observed in the absorption lines. A light-curve solution employing our new mass-ratio shows that the short-period binary is detached. The third body emits about 40% of the radiation from the system, and is probably a binary itself. The distance modulus for SZ Cam (=9.88) is in good agreement with that of its parent cluster NGC1502 (=9.71, Crawford 1994).

IU Aur is another triple system, although we are unable to find spectroscopic evidence for the tertiary. The close binary is semi-detached, with the secondary filling its Roche lobe. The distance modulus of the system is 11.0, which is in approximate agreement with that of the Aur OB1 association ($= 10.6 \pm 0.2$, Humphreys 1978).

We note that the current models for interacting massive binaries all assume case B mass transfer, in which the mass-loser becomes a Wolf-Rayet star. Case A mass-transfer models (in which the mass-loser fills its Roche lobe while still on the main-sequence) are required in order to see whether or not they can explain the observed properties of the interacting systems.

Key words: Stars - Stars: early-type - Stars: fundamental parameters - Stars: binaries: general - Stars: evolution

1 INTRODUCTION

One of the most pressing problems in O star astrophysics is the so-called *mass discrepancy* between *spectroscopic* masses and *evolutionary* masses. The *spectroscopic* mass for a single star may be derived by means of detailed fitting of model atmospheres to high-dispersion spectra of the star in order to determine its effective temperature and surface gravity. Then, by assuming a luminosity of the star, for example from its membership of a cluster or association with a well-established distance, the mass of the star may be estimated. The *evolutionary* mass is that mass which the star should have according to evolutionary models when the star is placed in the HR diagram at the effective temperature and luminosity derived from the spectroscopic analysis. Line-blanketed model atmospheres seem to be resolving, or at least ameliorating, the problem (Hubeny 1997), with a significant (2000 K) reduction in the effective temperatures over previous unblanketed models. In truth, this discrepancy may only be addressed rigorously by using detached, eclipsing, double-lined spectroscopic binaries, which allow an accurate determination of masses, radii, and (to a lesser degree for early-type stars) temperatures and luminosities.

Unfortunately detached O+O systems (with short enough periods to make spectroscopic radial velocity measurements and complete light-curves practicable) are relatively rare; the brevity of the main-sequence lifetimes means that we often observe O+O systems in the post mass-transfer stage of evolution. Such systems are still of astrophysical interest, since interacting O+O binaries provide one evolutionary path to Wolf-Rayet stars.

The present situation with regard to the accurate determination of masses and other astrophysical parameters for O+O star binaries has recently been reviewed by Harries & Hilditch (1997), where some excellent agreements are to be found between empirical data on detached, unevolved binaries and the evolutionary models. This paper presents details on the observations and the data analyses on three more O+O binaries that we have studied as part of an ongoing investigation of the properties of O+O binary systems (cf. Hilditch, Harries & Bell 1996, Harries, Hilditch & Hill 1997, Harries & Hilditch 1997).

2 THE SPECTROSCOPY

All the spectra were obtained by GH between 1988 and 1993 at the Dominion Astrophysical Observatory by using the 1.2-m coudé spectrograph (3231 configuration) and a Reticon detector. The data cover the wavelength range 4000–4500Å with a reciprocal linear dispersion of 0.3Å px^{-1}. The resolution of the observations is typically $70\,\mathrm{km\,s^{-1}}$. The spectra were extracted, wavelength calibrated and heliocentric corrected by using the REDUCE package (Hill 1982).

The final dataset comprised 26 spectra of LZ Cep, with a typical signal-to-noise ratio (per pixel) of ~ 40, 21 spectra of SZ Cam (S/N$\sim$40) and 13 spectra of IU Aur (S/N$\sim$ 20).

3 LZ CEP

LZ Cep (=HD209481) is a bright ($V = 5.6$) double-lined, eclipsing spectroscopic binary which has been classified as O9.5V+O9.5V (Petrie 1962) and O8.5III+O9.5V (Conti & Alschuler 1971). It is thought to be a member of the Cep OB2 association, which has a distance modulus of 9.9 (Garmany & Stencel 1992). The magnitude difference of the components, estimated in the photographic region, appears to be around 0.5^{m} (Petrie 1962) or 0.6^{m} (Conti & Alschuler 1971) and the light-curve displays low amplitude ($\Delta m < 0.1^{\mathrm{m}}$) ellipsoidal variations (Hill, Hilditch & Pfannenschmidt 1976).

Four-colour photometry of LZ Cep was presented by Crawford et al. (1971) and using the relation

$$c_0 = -0.116 + 0.097(b-y)_0 \tag{1}$$

that is applicable to the O stars (Crawford 1973), and the relation

$$E(b-y) = E(c_1)/0.20 \tag{2}$$

(Crawford & Mandwewala 1976), we may solve iteratively for $E(b-y)$ and c_0. We find $c_0 = -0.128$, which is consistent with the late-O spectral classification (Crawford 1975), and $E(b-y) = 0.251$. Using the relation $E(b-y) = 0.777E(B-V)$ (Crawford & Mandwewala 1976) we obtain $E(B-V) = 0.32$ which is rather lower than the Cep OB2 reddening of 0.59 ± 0.19 derived from 32 stars by Garmany & Stencel (1992), although it does fall within their range (0.29–1.12).

Hilditch (1974) employed an oscilloscope comparator to measure the radial velocity variations of LZ Cep from photographic plates. He determined semi-amplitudes of $98 \pm 3.1\,\mathrm{km\,s^{-1}}$ and $207.4 \pm 3.2\,\mathrm{km\,s^{-1}}$ for the primary and secondary respectively. A second study of the RV variations (Howarth et al. 1991) used high-resolution *IUE* spectroscopy combined with cross-correlation procedures. It was discovered that the Hilditch measurements were affected by absorption-line blending problems, and that the secondary semi-amplitude was significantly larger than the Hilditch measurement ($89 \pm 1.3\,\mathrm{km\,s^{-1}}$ and $232.9 \pm 1.7\,\mathrm{km\,s^{-1}}$). Two models of the binary configuration were presented: The first assumed a contact geometry, but this model yielded $\Delta B = 1.0$, which is inconsistent with the spectroscopy. A semi-detached configuration, with the less massive star filling its Roche lobe, was more consistent with the observations, and although no light-curve solution was performed the light variations derived from the model were shown to be in adequate agreement with the ellipsoidal V-band light-curve of Hill, Hilditch & Pfannenschmidt (1976).

Table 1. Equivalent width measurements for LZ Cep. Listed are the line wavelength, the species, and the equivalent widths (in Å) of the line for the primary and secondary respectively.

Wavelength (Å)	Species	Prim. EW (Å)	Sec. EW (Å)
4026	He I	0.47 ± 0.04	0.31 ± 0.05
4143	He I	0.14 ± 0.01	0.17 ± 0.01
4199	He II	0.24 ± 0.02	0.08 ± 0.02
4388	He I	0.21 ± 0.02	0.21 ± 0.02
4471	He I	0.56 ± 0.02	0.29 ± 0.02

3.1 The spectral types and the light-ratio

We constructed a mean quadrature spectrum by summing three spectra taken close to photometric phase 0.25. We then measured the equivalent widths of the strongest lines in the spectrum by fitting two component Gaussians (see Table 1).

An empirical calibration of equivalent width against spectral-type for the different lines (see Hill et al. (1994) and references therein) was used to construct a light-ratio/spectral-type diagnostic diagram: We divided the empirical EW of each line and spectral type by the appropriate measured EW taken for Table 1 and then plotted this ratio as a function of spectral-type for each line (see Figure 1). The diagnostic lines cross at a spectral type of O8.5 for the primary and O9.5–B0 for the secondary, in broad agreement with the spectral types of Conti & Alschuler. The intersection occurs at a ratio of 1.65 ± 0.1, and this corresponds to $(l+1)$ where l is the light ratio (primary/secondary). Hence we find a light ratio of 0.65 ± 0.1 or $\Delta M = 0.5 \pm 0.2$ (in approximately the B band), in good agreement with the estimates of Petrie (1962) and Conti & Alschuler (1971).

3.2 Radial velocities

The radial velocities were measured by using cross-correlation. A spectrum of 10 Lac was used as the template, and the Hδ and Hγ lines were excluded from the

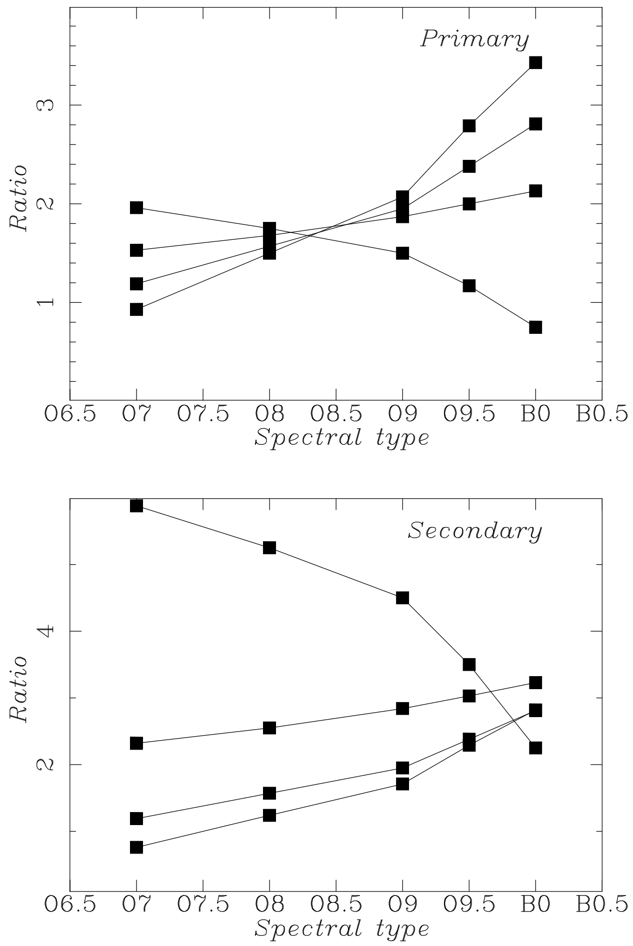

Figure 1. The ratio of empirical to observed equivalent widths for the helium lines of LZ Cep. The upper and lower panels refer to the primary and secondary stars respectively. The He II λ4199 line has a negative slope in both figures.

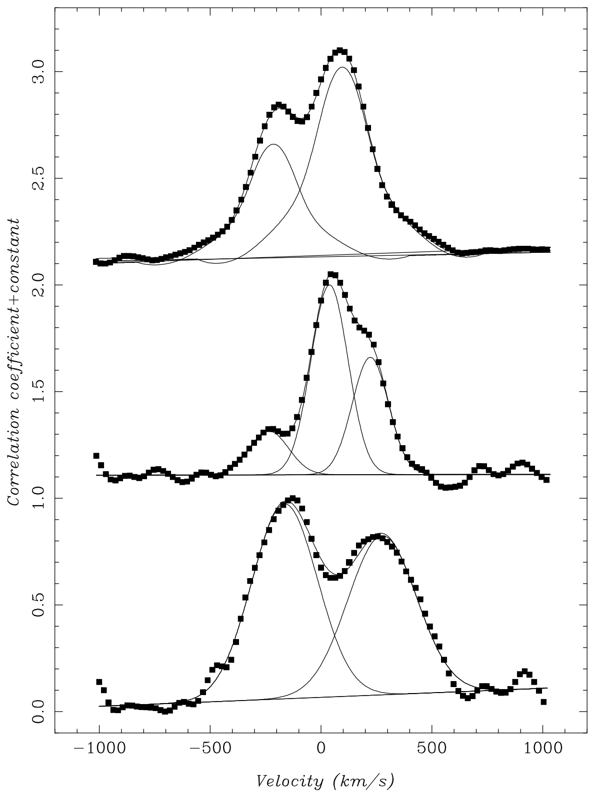

Figure 2. Sample cross-correlation functions for the three binaries (filled squares) along with their fits from the cross correlation analysis (solid lines). The individual components of the fits are also plotted. The CCFs are for LZ Cep, SZ Cam and IU Aur (top to bottom).

cross-correlation calculation. The cross-correlation function (CCF) peaks were well separated at quadrature, and were fitted by using a digital profile constructed from the auto-correlation function of a template spectrum, artificially broadened by a 100 km s^{-1} rotational broadening function. The fits to the CCF at quadratures was generally excellent (see for example Figure 2), and it was found that the FWHM of the two digital profiles was constant to with $\pm$20 km s^{-1}. For the more blended CCFs the FWHM of the fitting functions were fixed to the mean values derived from the quadrature fits (310 km s^{-1} and 245 km s^{-1} for the primary and secondary respectively).

We found no evidence, either in the spectra or in the CCFs, for a strengthening of the spectral features of either component when the star is appoaching (the Struve-Sahade effect).

The measured velocities are listed in Table 2, along with the non-Keplerian corrections required by the photometric solution (see Section 3.3). We solved the RV curve by using the RVORBIT program (Hill 1986), fixing the period at 3.070507d (Howarth et al. 1991) and solving for systemic velocity, the two semi-amplitudes, the eccentricity, the longitude of periastron and the time of periastron. The resulting eccentricity ($e = 0.017 \pm 0.084$) was insignificant, so we adopted a circular orbit, fitting for the systemic velocity, the two semi-amplitudes and the time of maximum positive velocity of the primary. The results of the fit are listed in Table 3 and the fit is illustrated in Figure 3.

We note that the semi-amplitude of the primary (94.6 ± 1.1 km s^{-1}) is slightly larger than that found by Howarth et al. (89.0 ± 1.3 km s^{-1}), but the semi-amplitude of the secondary is in excellent agreement with their value. Howarth et al. found an statistically significant eccentricity of 0.0310 ± 0.0068 from their *IUE* radial velocity curve, which had better phase coverage than that presented here. One possible explanation is that the Howarth et al. measurements (which were made using Gaussian fits to the CCFs rather than digital profiles) are affected by systematic errors due to blending at conjunction phases, which may introduce a spurious eccentricity. We stress that the derived semi-amplitudes from the two RV curves are in good agreement, despite this small discrepancy in the orbital eccentricity.

Table 3. Radial velocity curve solutions.

Parameter	LZ Cep	SZ Cam	IU Aur
γ ($\mathrm{km\,s^{-1}}$)	-2.4 ± 0.9	-12 ± 3	9 ± 5
K_1 ($\mathrm{km\,s^{-1}}$)	94.6 ± 1.1	225.8 ± 3.8	162.7 ± 6.8
K_2 ($\mathrm{km\,s^{-1}}$)	228.0 ± 1.1	259.1 ± 4.0	324.3 ± 5.9
$q(p/s)$	2.412 ± 0.032	1.148 ± 0.026	1.993 ± 0.091
P (d)	3.070507	2.698393	1.811474
$T_{\max}$	2446650.388 ± 0.0053	2445634.145 ± 0.014	2447787.913 ± 0.021

Table 2. Radial velocity measurements of LZ Cep. The phase (ϕ) is quoted with respect to the time of maximum positive velocity of the primary. The primary (v_1) and secondary (v_2) radial velocities are listed, along with the non-Keplerian velocity corrections (δv_1 and δv_2) which must be subtracted from the measurements. All velocities are in $\mathrm{km\,s^{-1}}$.

HJD (−2400000)	ϕ	v_1	δv_1	v_2	δv_2
46677.891	0.642	81	−1.05	−221	3.79
46677.934	0.298	87	−1.07	−225	4.23
46740.700	0.974	−89	0.62	182	−3.63
46740.707	0.975	−91	0.64	189	−3.67
46742.631	0.128	96	−0.70	−215	3.77
46742.691	0.479	86	−0.50	−209	3.38
46782.606	0.349	93	−0.50	−204	3.39
46794.675	0.076	85	−1.05	−225	4.25
46794.685	0.489	98	−1.04	−223	4.23
46326.885	0.490	−62	0.27	135	1.88
46328.901	0.535	−25	−0.15	67	−1.02
46367.821	0.536	87	−1.07	−226	4.27
46367.826	0.957	92	−1.07	−227	4.29
46972.952	0.971	78	−0.59	−221	3.57
46972.954	0.413	88	−0.58	−219	3.56
46973.968	0.415	−76	0.32	158	−2.94
46975.877	0.042	87	−0.99	−229	4.17
46975.880	0.061	85	−0.98	−230	4.16
46386.717	0.061	65	0.06	−151	1.71
46387.795	0.991	−100	1.07	217	−4.32
46442.666	0.994	−53	0.04	118	−2.05
46475.603	0.052	85	−0.35	−190	3.02
46645.749	0.053	−89	1.07	232	−4.27
46645.752	0.383	−94	1.07	226	−4.26
46648.960	0.005	−90	0.92	227	−2.50
46648.965	0.006	−92	0.91	221	−2.44

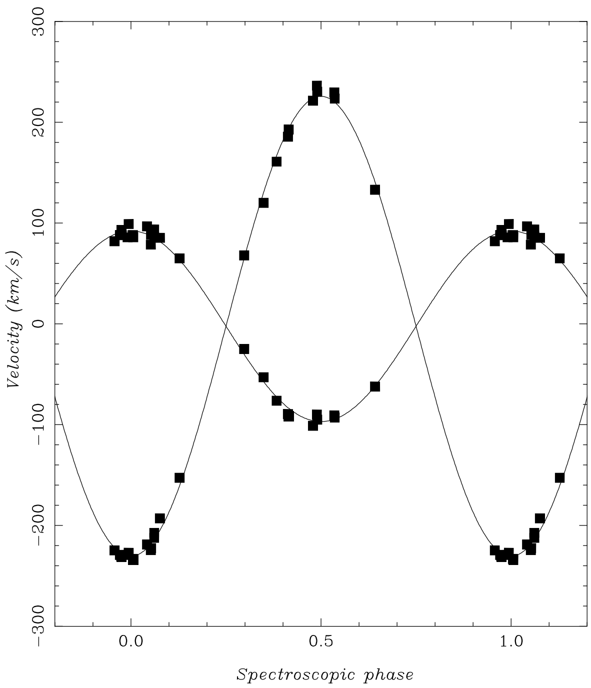

Figure 3. Radial velocity curve of LZ Cep. The phase is plotted with respect to the time of maximum positive velocity of the primary.

3.3 The light-curve solution

We employed the three-colour photoelectric light-curves of Hill, Hilditch & Pfannenschmidt (1976), which were obtained using a 16-inch telescope and a four-channel photometer. We included additional observations obtained using the same instrument, but which were unpublished in the original paper. (For completeness we list the photometry in Table 4.) The phase of the light-curve was obtained by using the spectroscopic period found by Howarth et al. (1991) (3.070507d) and a time of primary minimum found from a parabolic fit to the b light-curve ($T_{min} = 2441897.9787$).

We used the LIGHT2 program (Hill 1979; Hill & Rucinski 1993) to solve the light-curve. We adopted mean temperatures of 32 000K and 30 000 for the primary (O8.5) and secondary (O9.5) stars respectively, following the spectral-type–$T_{\rm eff}$ calibration of Böhm-Vitense (1981) and applying the corrections derived by Hilditch, Harries & Bell (1996). The magnitude difference between the components was fixed at $0.5^{\rm m}$ at 4400Å (approximately the B-band).

It was found that neither a contact nor a detached configuration could satisfy the constraints of the light-curve while maintaining the measured light ratio. We agree with Howarth et al. that a semi-detached configuration, with the secondary filling its Roche lobe, is the best model for the system. We solved the light-curve, fitting the three colours simultaneously and holding the mean temperatures fixed with the secondary filling its Roche lobe. Since the magnitude difference is fixed, the only free parameter in the light-curve solution was the inclination. The light-curve fit is illustrated in Figure 4 and the photometric parameters are listed in Ta-

Table 4. Photometry of LZ Cep.

HJD (−2440000)	Δ(35)	Δ(44)	Δ(55)	HJD (−2440000)	Δ(35)	Δ(44)	Δ(55)	HJD (−2440000)	Δ(35)	Δ(44)	Δ(55)
1161.9097	0.948	1.144	0.988	1536.8979	1.008	1.236	1.091	1936.9180	0.979	1.165	1.015
1161.9192	0.953	1.146	0.978	1536.9019	1.018	1.199	1.048	1938.7925	0.982	1.163	1.016
1162.9236	1.010	1.198	1.031	1557.9648	0.948	1.146	0.982	1938.7949	0.969	1.153	0.994
1162.9309	0.990	1.185	1.021	1557.9744	0.956	1.147	0.989	2243.8420	0.968	1.167	1.014
1163.9312	1.020	1.212	1.053	1558.7625	1.039	1.225	1.069	2243.8505	0.969	1.162	1.012
1163.9390	1.017	1.210	1.047	1558.7666	1.051	1.236	1.080	2259.8120	0.965	1.164	1.010
1164.9353	0.951	1.143	1.000	1558.9446	1.012	1.201	1.044	2259.8153	0.982	1.171	1.015
1164.9458	0.973	1.162	0.986	1558.9490	1.022	1.212	1.060	2259.9214	0.985	1.181	1.024
1165.9377	1.016	1.205	1.054	1560.8474	0.973	1.155	0.995	2259.9248	0.980	1.178	1.021
1165.9441	1.002	1.199	1.035	1560.9436	0.961	1.145	0.993	2266.8324	0.969	1.175	1.017
1167.9336	0.940	1.135	0.991	1560.9478	0.961	1.151	0.996	2266.8370	0.964	1.166	1.010
1167.9421	0.934	1.144	0.991	1851.9158	1.039	1.234	1.080	2266.8405	0.981	1.175	1.023
1168.9302	1.008	1.201	1.042	1851.9199	1.030	1.209	1.050	2267.9163	1.009	1.209	1.058
1168.9375	1.002	1.199	1.061	1858.8704	0.962	1.151	0.991	2267.9194	1.018	1.211	1.066
1169.9397	0.989	1.189	1.036	1858.8752	0.958	1.152	0.988	2268.9585	0.946	1.149	0.992
1169.9468	0.990	1.191	1.037	1860.9102	1.030	1.216	1.064	2268.9617	0.959	1.155	0.999
1170.9353	0.956	1.150	0.980	1860.9143	1.022	1.212	1.064	2275.8775	1.001	1.203	1.043
1170.9443	0.944	1.133	0.987	1879.8975	1.022	1.209	1.049	2275.8819	1.001	1.206	1.045
1171.9539	1.032	1.221	1.058	1879.9004	1.020	1.205	1.043	2276.8482	0.991	1.185	1.027
1171.9617	1.004	1.207	1.060	1887.8662	0.976	1.159	0.992	2276.8528	0.991	1.190	1.031
1172.9409	0.992	1.189	1.021	1887.8696	0.969	1.152	0.989	2284.9237	1.037	1.233	1.081
1172.9473	0.990	1.187	1.020	1890.9553	0.967	1.154	0.999	2284.9305	1.037	1.234	1.077
1175.9197	0.982	1.167	1.015	1890.9592	0.960	1.154	1.002	2289.9215	0.963	1.163	1.015
1175.9285	0.948	1.164	1.009	1896.8328	0.987	1.179	1.023	2289.9247	0.970	1.176	1.015
1176.8950	0.992	1.177	1.015	1896.8374	0.991	1.181	1.022	2290.8676	1.034	1.227	1.070
1176.9072	0.982	1.165	1.005	1897.8782	1.048	1.230	1.078	2290.8728	1.029	1.223	1.067
1180.9045	1.009	1.222	1.060	1897.8813	1.045	1.234	1.075	2292.8668	0.989	1.187	1.034
1180.9141	1.024	1.223	1.055	1903.9055	1.026	1.212	1.049	2292.8712	0.990	1.193	1.032
1182.9333	1.013	1.192	1.032	1903.9089	1.022	1.209	1.050	2293.8665	1.016	1.213	1.059
1184.9531	0.942	1.140	0.984	1906.8684	1.011	1.202	1.041	2293.8707	1.018	1.211	1.060
1184.9590	0.964	1.160	0.998	1906.8728	1.018	1.203	1.038	2572.9233	0.973	1.157	0.990
1211.8042	1.028	1.220	1.063	1911.9185	1.028	1.217	1.063	2572.9287	0.962	1.142	0.991
1217.8801	1.027	1.220	1.062	1911.9219	1.034	1.217	1.069	2572.9299	0.960	1.147	0.988
1499.7747	0.939	1.146	0.985	1912.9290	1.001	1.194	1.031	2602.9309	1.002	1.201	1.042
1499.7793	0.939	1.127	0.988	1912.9324	0.998	1.185	1.029	2602.9361	1.008	1.201	1.034
1501.8042	1.113	1.267	1.109	1926.9294	1.030	1.216	1.058	2603.9318	1.022	1.219	1.044
1501.8096	1.123	1.270	1.104	1926.9377	1.029	1.209	1.055	2603.9369	1.016	1.209	1.041
1515.9314	1.028	1.219	1.064	1927.8926	0.970	1.147	1.004	2636.9066	0.973	1.166	1.019
1518.9326	1.044	1.227	1.067	1927.8960	0.974	1.152	0.993	2636.9119	0.962	1.165	1.009
1518.9387	1.054	1.219	1.065	1929.8491	1.013	1.197	1.029	2637.9005	1.041	1.236	1.056
1526.8718	0.991	1.178	1.025	1929.8521	1.012	1.192	1.031	2637.9148	1.045	1.237	1.065
1526.8772	0.994	1.168	1.031	1931.8665	1.072	1.252	1.091	2638.8687	0.954	1.159	0.972
1527.8250	1.038	1.226	1.061	1931.8704	1.059	1.241	1.089	2638.8897	0.942	1.147	0.973
1527.8313	1.028	1.213	1.064	1935.9785	1.009	1.193	1.038	2639.9374	0.980	1.179	1.015
1530.8730	1.025	1.207	1.057	1935.9822	0.985	1.187	1.041	2639.9422	1.005	1.189	1.011
1530.8782	1.021	1.207	1.054	1936.9146	0.986	1.170	1.022				

ble 5. Although the light-curve solution assumed a circular orbit, we note that a light-curve fit adopting the eccentricity and longitude of periastron found by Howarth et al. (1991) yielded a poorer fit and a higher inclination ($i = 56°$). There is no evidence from the photometry that the secondary minimum occurs before $\phi = 0.5$.

Since the secondary star in LZ Cep is tidally distorted, the velocity of the centre of light of the star is not the star's centre of mass. We therefore applied so-called non-Keplerian corrections to the measured RVs (these are listed in Table 2) before determining the RV solution. This resulted in a slightly different mass-ratio, which was then used to compute a new light-curve solution and hence revised non-Keplerian corrections. Two iterations of this procedure were required for convergence between the light curve and RV curve solutions.

3.4 The physical parameters

Combining the RV and light-curve solutions were are able to determine the physical parameters of the components of LZ Cep (see Table 6). We find a distance modulus to LZ Cep (taking the reddening from §3.1) of 9.6±0.2, which is slightly smaller than the distance modulus to Cep OB2 (=9.9, Gar-

Table 5. Light curve solution parameters. The value of $\bar{r}$ is the mean (equivalent volume) radius relative to the binary separation and $T_{\rm eff}$ refers to the mean effective temperature. The asterix (*) denotes a Roche lobe filling star.

	LZ Cep		SZ Cam			IU Aur		
Parameter	p	s	p	s	t	p	s	t
$\bar{r}$	0.3635 ±0.0074	*0.3061	0.3187 ±0.0098	0.2972 ±0.0120	0.2700	0.3534 ±0.0048	*0.3270	0.3100
$T_{\rm eff}$ (K)	31 888 ±500	30 051 ±500	29 725 ±500	27 183 ±523	29 784 ±2810	29 825 ±500	26 830 ±100	20 626 ±745
i (°)	52.6 ± 0.5		76.9 ± 0.4			88.0 ± 0.5		

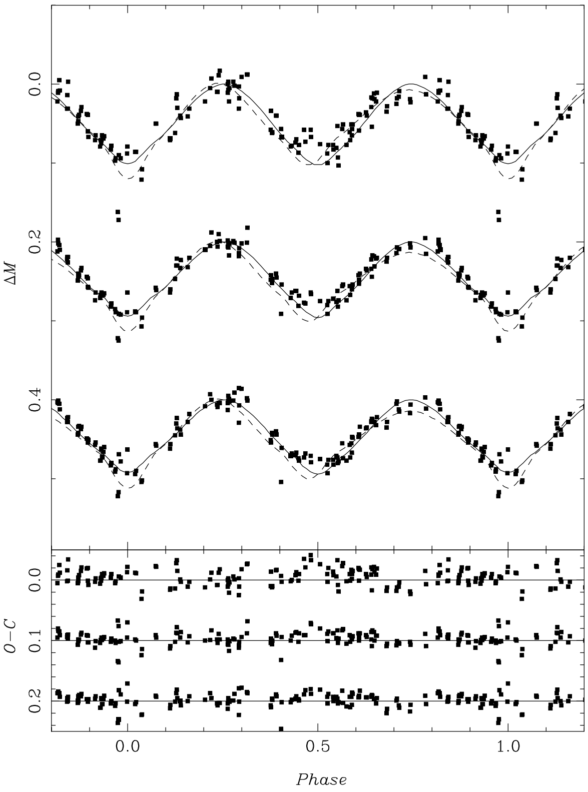

Figure 4. Photometry of LZ Cep. The U (top) B (middle) and V (bottom) light-curves (see Table 4) are plotted together with the best-fit solutions assuming a circular orbit (solid lines) and the best-fit adopting the eccentricity of Howarth et al. (1991) (dashed line). The lower panel shows the $(O-C)$s of the circular orbit light-curve fit.

many & Stencel 1992). The projected rotational velocities we derive ($117 \pm 3\,{\rm km\,s^{-1}}$and $99 \pm 1\,{\rm km\,s^{-1}}$) are in satisfactory agreement with those measured by Howarth et al. (1997) from cross-correlation ($138\,{\rm km\,s^{-1}}$and $92\,{\rm km\,s^{-1}}$).

Comparing our parameters to those derived by Howarth et al. (1991), we see that our results give stars that are less massive, smaller, and less luminous. It should be remembered that the Howarth et al. parameters are not based on a solution to the light-curves, but instead rest on the assumption of cluster membership (to give M_V), adopted temperatures of 34 000K for both stars, a magnitude difference of $\Delta M = 0.55$, and the assumption of a semi-detached configuration. We believe that their adopted temperatures are probably too hot, and that the primary is considerably ($\sim$ 2000K) hotter than the secondary, and a recent estimate of the UV magnitude difference ($0.7^{\rm m}$, Howarth et al. 1997) supports this assertion. We also suggest that the absolute magnitude calibration of the O stars is not precise enough to provide accurate radii.

4 SZ CAM

The eclipsing system SZ Cam (=HD25638) is the brightest object of the open cluster NGC1502 (e.g. Crawford 1994). The primary was classified as O9.5V by Budding (1975).

Mayer et al. (1994) identified the system as a triple, composed of a close binary (P = 2.7d) orbiting a massive companion (P = 50.7yr). Light-travel effects have led to periodic changes in the times of minima, which were initially interpreted as changes in the 2.7d orbital period (Chochol 1977). Mayer et al. (1994) showed that high-resolution spectroscopy was capable of resolving the Hα absorption profile into three components, and significant velocity changes could been seen in the tertiary component of the line. They estimated the minimum mass of the tertiary component as $18.6\,{\rm M_\odot}$ and proposed that the tertiary body is actually a close binary. The system has been resolved by speckle interferometry, with the tertiary separated from the 2.7d binary by 0.07 arcsec (Mason et al. 1997).

4.1 Radial velocities

The radial velocities of SZ Cam were measured by using cross-correlation. A synthetic template spectrum was used, since the the three peaks in the CCF could not be resolved using a standard stellar spectrum. The synthetic template consisted of narrow ($50\,{\rm km\,s^{-1}}$) Gaussian absorption line profiles at λ4026, λ4143, λ4187 and λ4388. A three component Gaussian fit to the asymmetric CCF normally yielded a satisfactory fit, with the FWHM of the three Gaussians approximately constant with orbital phase. For the very

Table 6. Astrophysical parameters of the program stars obtained by combining the spectroscopic orbit and light-curve solutions. The primary, secondary and tertiary components are labelled as p, s and t respectively. Volume equivalent radii and mean effective temperatures are quoted.

	LZ Cep		SZ Cam			IU Aur		
Parameter	p	s	p	s	t	p	s	t
Spec. type	O8.5	O9.5	O9.5	B0		B0.5	B0.5	
Mass ($M_\odot$)	15.1 ±0.4	6.3 ±0.2	18.5 ±0.7	16.1 ±0.6		14.5 ±0.7	7.3 ±0.5	
Radius ($R_\odot$)	9.0 ±0.2	7.5 ±0.1	8.5 ±0.3	7.9 ±0.3	7.2 ±0.1	6.2 ±0.1	5.7 ±0.1	5.3 ±0.1
$T_{\rm eff}$ (K)	31 881 ±500	30 057 ±500	29 725 ±500	27 183 ±523	29 784 ±2810	29 825 ±500	26 830 ±100	20 626 ±724
$\log g$ (dex)	3.71 ±0.02	3.48 ±0.02	3.85 ±0.03	3.85 ±0.04		4.01 ±0.03	3.79 ±0.04	
$M_{\rm bol}$	−7.54 ±0.08	−6.91 ±0.07	−7.11 ±0.10	−6.57 ±0.10	6.67 ±0.10	−6.44 ±0.09	−5.81 ±0.04	−4.42 ±0.05
M_V	−4.41 ±0.09	−3.93 ±0.09	−4.16 ±0.11	−3.88 ±0.14	−3.72 ±0.20	−3.48 ±0.10	−3.16 ±0.05	−2.30 ±0.10
$\log(L/L_\odot)$	4.90 ±0.03	4.65 ±0.03	4.73 ±0.04	4.52 ±0.05	4.56 ±0.04	4.36 ±0.04	4.21 ±0.02	3.66 ±0.05
$v_{\rm rot} \sin i$ ($\rm km\,s^{-1}$)	117 ±3	99 ±1	154 ±5	144 ±6		172 ±4	159 ±3	

blended cases it was necessary to fix the FWHM of the Gaussians to their mean values taken from the well resolved CCFs. Typically all three CCF peaks were resolved, although in a few cases only one or two of the Gaussian fits yielded reliable velocities. A typical fit to the CCF is displayed in Figure 2, while the velocities of the primary, secondary and tertiary components are listed in Table 7. The formal errors on the Gaussian fits were $\sim 10\,\rm km\,s^{-1}$. Gaps in Table 7 correspond to CCF fits that were clearly poor (primarily due to blending) and yielded unreliable velocities. No evidence of the Struve-Sahade effect was found in the spectra of CCFs.

The tertiary velocities measurements for 1990 Nov have a mean of $32 \pm 9\,\rm km\,s^{-1}$ and are constant (to within the errors) over this period. The 1991 Sep velocities have a mean of $-41 \pm 17\,\rm km\,s^{-1}$, and are again constant to within the measurement errors. There is a significant ($73 \pm 19\,\rm km\,s^{-1}$) change in velocity between the two epochs, which may be the result of either orbital motion of the tertiary or a systematic error in the velocity measurements. If the tertiary is indeed a non-eclipsing short-period binary then velocity changes in the tertiary absorption components are expected. Alternatively it is possible that our fits to the CCF peaks are affected by blending, which would explain the change in sign of the tertiary velocity between the first and second quadratures of the short-period binary, but if this was the case then such systematic effects might be evident in the RV measurements of the primary and secondary, which appear consistent (see Figure 5). Additional observations are required to resolve this problem, with either the temporal resolution to examine the change in the tertiary velocity through one orbital cycle of the short-period binary, or a long enough time series to search for a periodic change in the tertiary velocity.

A circular orbit fit (see Table 3) was made to the to the measured RVs, fixing the period at 2.698393d (Mayer et al. 1994) and solving for the time of maximum positive velocity and the two semi-amplitudes. The fit (see Figure 5 and Table 3) yielded semi-amplitudes of $225.8 \pm 3.8\,\rm km\,s^{-1}$ and $259.1 \pm 4.0\,\rm km\,s^{-1}$ for the primary and secondary components respectively. The primary semi-amplitude differs considerably from that quoted by Mayer et al. (1994) based on a preliminary analysis of their spectra.

4.2 Colour indices

Crawford (1994) has discussed the published $uvby\beta$ photometry of stars in NGC 1502 and concluded that the interstellar reddening to the cluster is $E(b-y) = 0.54^{\rm m}$, and its distance modulus is $V - M_V = 9.71$. The $uvby$ photometry of SZ Cam, observed outside eclipses by Hilditch & Hill (1975), provide mean values of $(b-y) = 0.431, m_1 = -0.107, c_1 = 0.002$. Using the standard relationships and intrinsic colours given in Crawford (1973, 1978, 1994), we obtain for SZ Cam, $(b-y)_0 = -0.124, c_0 = -0.109$, and $E(b-y) = 0.547$. The reddening value is in excellent agreement with that for the cluster as a whole, and the intrinsic colours are entirely consistent with the O9–B0 main sequence stars, as is the value of $\beta = 2.597$ (Hauck & Mermilliod 1980) according to Crawford (1978). These agreements with Budding's (1975) spectral classification of O9.5V for the primary component, the evidence for late-O spectral features for the tertiary, and with the cluster reddening, allow us to conclude that we may assign temperatures of 30 000 K for the primary and the tertiary components.

Table 7. Radial velocity measurements of SZ Cam. The phase (ϕ) is quoted with respect to the time of maximum positive velocity of the primary star. The primary (v_1), secondary (v_2), and tertiary (v_3) radial velocities are listed. All velocities are in km s^{-1}.

HJD (−2400000)	ϕ	v_1	v_2	v_3
48213.686	0.927	220	−235	38
48213.713	0.937	213		45
48213.744	0.949	194	−256	19
48213.772	0.959	215		38
48213.802	0.970	210	−262	32
48213.831	0.981	225	−284	40
48213.862	0.992	224	−282	37
48213.892	0.003	218	−259	33
48213.946	0.024	198	−266	21
48213.990	0.040	219	−256	36
48214.019	0.051	197	−238	30
48214.048	0.061	194	−277	18
48214.075	0.071		−237	
48519.967	0.429	−233	200	−59
48519.981	0.434	−191	228	−14
48519.999	0.441	−215	208	−41
48520.016	0.447	−223	242	−36
48946.617	0.537		237	
48946.633	0.543		264	
48946.793	0.602		193	
49043.700	0.514	−239	228	−53

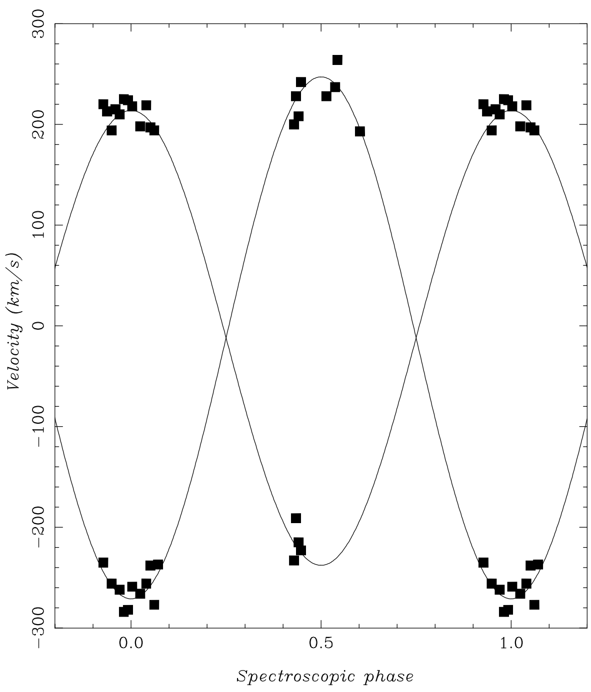

Figure 5. Radial velocity curve of SZ Cam. The phase is plotted with respect to the time of maximum positive velocity of the primary ($\phi = 0$).

4.3 Solutions of the light curves

Previous solutions of published light curves (see Chochol 1980, and references therein) have been marred by the use of an incorrect mass ratio for the system (e.g. Chochol derived $q = m_1/m_2 = 4.05$). Our revised mass ratio of $q = 1.148$ immediately permits the obvious interpretation of the light curves, with their nearly equal eclipse depths and small 'ellipticity' effects, as being those of a detached eclipsing system.

We have analysed the two light curves published by Chochol (1980), obtained with a photoelectric photometer and intermediate-band filters centred on 472nm and 572nm, both with half-widths of 19.5nm, hereafter referred to as the b and y light curves. The b and y measurements were not contemporaneous, and the number of published normal points per unit phase interval is limited, so we were unable to fit least-squares cubic splines to the two sets of data and derive b and y light curves interpolated to the same intervals of orbital phase. Accordingly, we solved each curve independently, keeping the mass ratio fixed at the new spectroscopic value, and the temperature of the primary fixed at 30 000K. Solutions for the radii of the primary and secondary stars were made, together with the temperature of the secondary, the orbital inclination, and the contribution of the third light in the system. Third light is a necessary component in the system, since it is self-evident in our CCFs at $\sim 40\%$ of the total light of the system, its spectral features must resemble that of the CCF template, and the eclipse depths are too shallow to be consistent with the derived minimum masses and the observed spectral types. We found that the minimum value of reduced $\chi^2 = 1.000$ was achieved when the tertiary contributed 40% of the total light of the system, in agreement with the spectral information revealed by cross correlation.

The temperature of the tertiary is reasonably well-constrained by the presence of late-O type spectral features, but although we quoted a tertiary radius it is the *luminosity* of this component that is the important value, since the tertiary itself may be a double. The results are detailed in Table 5 while the fit is plotted in Figure 6.

4.4 The physical parameters

The non-Keplerian corrections were found to be negligible for this detached system. We combined the RV and light curve solutions to give the physical parameters listed in Table 6.

The third body contributes 40% to the total light of the system, consistent with the strength of the absorption lines. The total absolute visual magnitude of the system is −5.13. Taking $V = 6.94$ and $E(b - y) = 0.547$ we obtain a distance modulus, $V_0 - M = 9.88$, which is in good agreement with the distance modulus of NGC1502 (= 9.71) derived by Crawford (1994) from B-star calibrations.

5 IU AUR

IU Aur (=HD35652) is another triple system, comprising a B0.5+B0.5 (Mammano et al. 1977) semi-detached binary ($P = 1.9d$) and a gravitationally-bound tertiary ($P = 294d$)

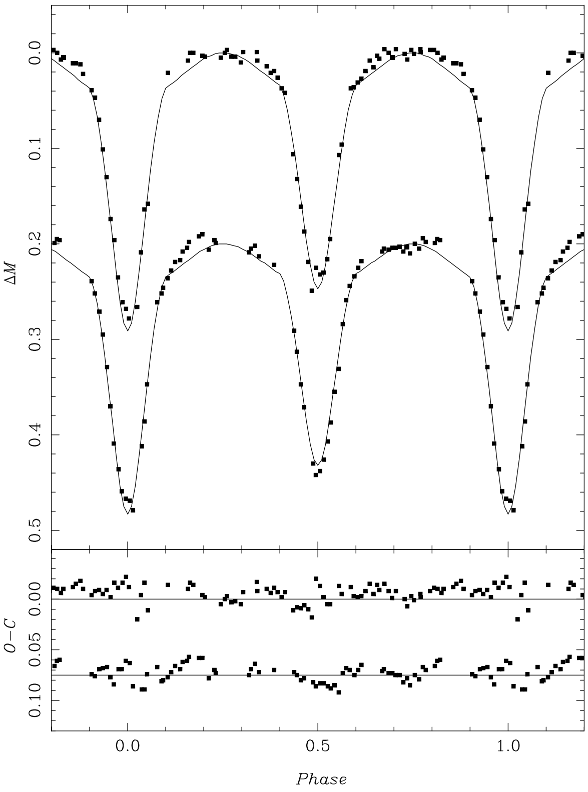

Figure 6. The b (top) and y (bottom) light-curves of SZ Cam (Chochol (1980), along with the light-curve solutions (solid lines) and the $(O-C)$s (bottom panel).

which contributes $\sim 15-25\%$ to the total radiation (Mayer & Drechsel 1987). Liu et al. (1988) found the orbital inclination of the binary to be increasing at a rate of 0.4° per year, although this value is somewhat uncertain since the inclination and the third-light contribution are strongly correlated in the light-curve solutions. A reversal in the depths of the eclipse minima was discovered by Ohmori (1989) and Mayer et al. (1991), and it has been calculated that the orbital plane passed through 90° inclination during 1984. A valuable summary of previous work on this system is given by Drechsel et al. (1994).

The system has been resolved by using speckle interferometry (Mason et al. 1997) and by Hipparcos (0.147 and 0.130 arcsec separation respectively). Such a large angular separation suggests a much longer period than that proposed for the tertiary by Mayer & Dreschel (1987), indicating that the system may be quadruple.

The spectral types for the components have ranged from O9V to B3V (Hill et al. 1975), and B0.5+B0.5 (Mammano et al. 1977). Our new spectra certainly confirm the B0 classification, with only marginal evidence for the presence of the He II λ4200 line. Of the 5 *uvby* measurements of IU Aur reported by Hilditch et al. (1975), 3 were obtained outside eclipses. The average values of colour indices are $(b-y)=0.239$, $m_1=-0.026$, and $c_1=-0.063$. A value of $\beta=2.635$ is also given by Hauck & Mermilliod (1980). Assuming a B0V classification, we may expect $(b-y)_0=-0.12$ (Crawford 1978). Then $E(b-y)=0.36$, and $c_0=-0.135$. This value of c_0 is bluer, by -0.07, than expected for a B0V star, but is close to that listed for a B0III star, for which Crawford (1978) gives $c_0=-0.10$. Our spectra would not admit a primary component of spectral type earlier than O9.5V, because of the weakness of the He II line, so the c_1 index is probably indicating the somewhat evolved status of the binary. The value of β is consistent with the sum of the slightly cooler secondary star, and the cooler tertiary (see section 5.2).

Drechsel et al. (1994) presented two high-resolution spectra of IU Aur, taken at opposite quadratures, which showed three components to the Hα absorption profile. (A three component structure to the He I λ6678 line is also claimed, but the evidence is rather less convincing.) The two spectra were used to determine velocities ($232.3\pm5.3\,\mathrm{km\,s^{-1}}$ and $342\pm21\,\mathrm{km\,s^{-1}}$), which seemed to confirm the mass ratio $q=m_1/m_2=1.47$ derived by Mammano et al. (1977) from an extensive radial velocity study of the system. That radial velocity study was based upon a large number of photographic spectra obtained at a reciprocal dispersion of $42\,\mathrm{\AA\,mm^{-1}}$, though the method used to determine the velocities was not reported. All the light curve solutions published to date have assumed the mass ratio to be 1.47.

5.1 Radial velocities

The radial velocities of IU Aur were measured by means of cross correlation against the synthetic template described in section 4.1. The spectra were searched carefully for evidence of absorption components attributable to a third body, not only with the above-mentioned template, but also with various templates of later spectral type. We were unable to find spectral evidence for the third body, and all the CCFs were double-peaked at all the observed orbital phases. With a third light contribution of $\sim 20\%$, derived from the light curves, it is possible that the third body absorption lines could remain hidden in the CCFs at low velocities relative to the systemic velocity of the binary.

The double-peaked CCFs were fitted by using two-component Gaussian profiles, which gave a satisfactory fit at all phases (see Figure 2). We found no evidence for the Struve-Sahade effect.The measured velocities (together with their associated non-Keplerian corrections) are listed in Table 8. The results of a circular-orbit solution to the RV curve, fixing the period at 1.811474d (Mayer & Drechsel 1987) is given in Table 3, and the fit is plotted in Figure 7. The semi-amplitudes of these new velocity curves are quite different from those reported by Mammano et al. (1977), due presumably to our data having significantly higher spectral resolution, more than a factor of 2, and to our improved techniques of measuring radial velocities. The mass ratio is therefore changed from 1.47 to 1.99.

We have studied the $(O-C)$ residuals between the observed velocities of both components and the values calculated according to our orbital solution for IU Aur. The data were obtained effectively at three epochs, separated by 276d and 758d. These residuals do not show clear evidence for any motion about a third body, but we note, in agreement with

Table 8. Radial velocity measurements of IU Aur. The phase (ϕ) is quoted with respect to the time of maximum positive velocity of the primary star. The primary (v_1) and secondary (v_2) radial velocities are listed, along with the non-Keplerian velocity corrections (δv_1 and δv_2) which must be subtracted from the measurements. All velocities are in $\mathrm{km\,s^{-1}}$.

HJD (−2400000)	ϕ	v_1	δv_1	v_2	δv_2
47511.755	0.551	−165	1.58	278	−7.10
47511.794	0.572	−146	1.55	300	−6.08
47511.875	0.617	−135	1.17	233	−2.25
47787.969	0.031	175	−1.58	−296	6.47
47787.995	0.045	164	−1.58	−313	7.07
47788.018	0.058	171	−1.50	−274	7.19
47788.840	0.512	−121	1.15	328	−6.44
47788.877	0.532	−150	1.44	333	−7.13
47788.908	0.549	−122	1.57	319	−7.14
47788.937	0.565	−130	1.57	300	−6.50
47853.006	0.934	178	−0.66	−252	−3.44
48546.879	0.977	103	−1.15	−338	2.07
48546.905	0.991	149	−1.30	−266	3.39

Mammano et al. that these (O-C) residuals are substantially larger than we would expect for the quality of spectra employed in this study. For LZ Cep, the average *rms* scatter over both components is $\pm 5\,\mathrm{km\,s^{-1}}$, whilst those for SZ Cam and IU Aur are respectively $\pm 14\,\mathrm{km\,s^{-1}}$ and $\pm 24\,\mathrm{km\,s^{-1}}$. The SZ Cam system is $\sim 1^{\mathrm{m}}$ fainter than LZ Cep, whilst IU Aur is $\sim 2.5^{\mathrm{m}}$ fainter.

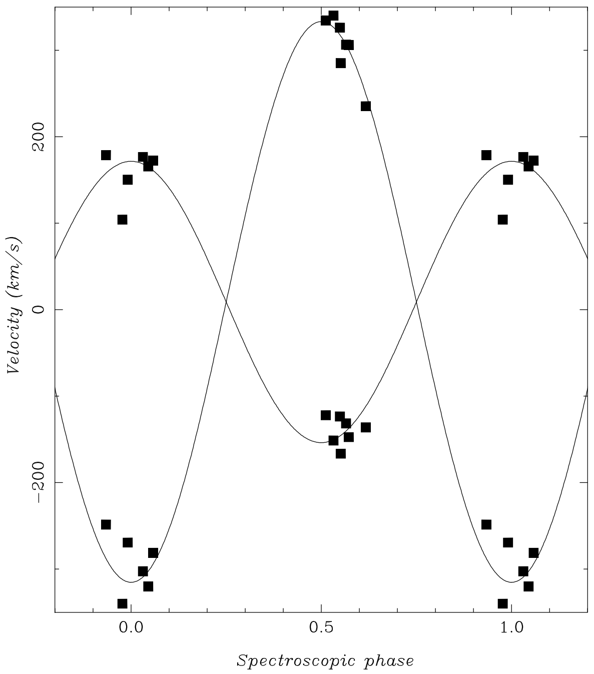

Figure 7. Radial velocity curve of IU Aur. The phase is plotted with respect to the time of maximum positive velocity of the primary ($\phi = 0$).

5.2 Solutions of the light curves

The *UBV* light curves obtained in 1984 by Mayer & Drechsel (1987) were solved by means of the LIGHT2 program. A mean temperature of 30 000K was adopted for the primary component, corresponding to the earliest possible spectral type of O9.5V, and we fixed the mass ratio at the newly determined value of 1.993. The third light contribution is described within the LIGHT2 code by a temperature (T_3), and a radius (r_3) given in terms of the semi-major axis of the relative orbit of the binary. We conducted a 'grid-search' over a range of tertiary radii and temperatures, and solving for the radii (r_1, r_2) of the primary and secondary components, the temperature(T_2) of the secondary, and the orbital inclination(i). Because we were solving the *UBV* light curves simultaneously, we could hope to find information about the third-body temperature in these data. The minimum χ^2 value in this grid occurred around $15\,000 \leq T_3 \leq 21\,000$, and $0.30 \leq r_3 \leq 0.35$. We also found that the light curves required a semi-detached configuration, with the secondary component filling its Roche lobe, thereby confirming previous investigations. Accordingly, we fixed the radius of the secondary component at the Roche lobe value appropriate to our newly determined spectroscopic mass ratio, and then solved the light curves for r_1, T_2, i, and T_3 at fixed values of r_3. The best fit solution to all three light curves gave the parameters listed in Table 5 with *rms* scatter about each of the three curves of $\leq 0.010^{\mathrm{m}}$. This third light contribution at quadrature amounts to 22% in V, 21% in B, and 16% in U, values that are in good agreement with previous investigations of these light curves, albeit with a different mass ratio. These values are also in excellent agreement with the magnitude difference measured by Hipparcos ($\Delta H_P = 1.36$), which suggests that the companion contributes 22% of the flux in the visible band.

5.3 The physical parameters

The final solutions of the light- and radial-velocity curves for IU Aur provide the astrophysical parameters listed in Table 6. We find masses for both components that are notably smaller than those derived by Drechsel et al., but these changes are due almost entirely to the revised values of the semi-amplitudes. The relative geometry of the system remains very similar, with IU Aur as a semi-detached binary, and a third body contributing about 20% of the total light of the system.

The absolute visual magnitude of the system ($M_V = -4.17$) combined with the maximum apparent visual magnitude ($V = 8.26$) and the reddening derived in §5 gives a distance modulus of 11.0. This is in approximate agreement with the distance modulus of the Aur OB1 association ($= 10.6 \pm 0.2$, Humphreys 1978), as is the interstellar extinction ($A_V = 1.45$ for IU Aur, compared to 1.4 ± 0.4 for the cluster found by Humphreys).

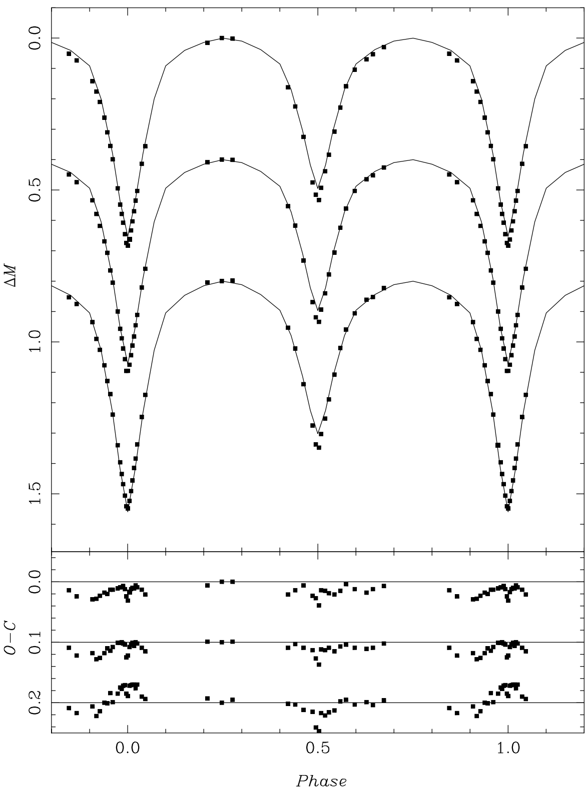

Figure 8. The U (top), B (middle) and V light-curves of Mayer & Drechsel (1987) along with the best-fit curves (solid lines). The lower panel shows the $(O-C)$s of the light-curve fit.

6 DISCUSSION

The results we have obtained for the detached system SZ Cam have been combined with those from other well-defined, detached and unevolved O+O binaries to investigate the agreements between these empirical data and the latest evolution models for single stars (see Harries & Hilditch 1997). We found that the values of masses, radii, and internal structure constants for stars in these detached systems are in excellent agreement with the models of Schaller et al. (1992) and Claret & Giménez (1992, 1993). Some revisions to the effective temperature scale would seem to be required, amounting to reductions of order 1–2000 K, dependent upon the spectral types of the stars concerned.

The semi-detached O+O binaries from this paper (LZ Cep and IU Aur), together with XZ Cep and V448 Cyg (Harries, Hilditch & Hill 1997), and AB Cru (Lorenz et al. 1994) are plotted in the mass–log g plane in Figure 9. All of these systems conform to our understandings about the evolution of close binaries through rapid mass-transfer phases, and thence to slow mass transfer phases. The mass losers are now seen as the less massive components that fill their respective Roche lobes, and are accordingly oversized and over-luminous relative to a ZAMS star of the same mass. The mass gainers are all still on the main sequence, and display a range of ages from 0–6 Myr that do not represent the ages of these interacting systems. When we make comparisons of these empirical results with theoretical models for the evolution of binary stars, we find that there is good qualitative agreement in general, except that most models have been calculated for case B mass exchange (i.e. Roche-lobe overflow for the mass loser occurring after core hydrogen exhaustion), rather than case A mass exchange (Roche-lobe overflow occurring during the main-sequence phase) (cf.,e.g., Vanbeveren & de Loore 1994; de Loore & Vanbeveren 1994a,b). Those case B models then predict that the mass losers should now be seen as Wolf-Rayet stars, which types of binaries are certainly to be found. But these 5 systems all have mass losers with normal late-O or early-B type spectra, which suggests that they are the products of case A mass exchange, rather than case B. We request that appropriate case A models should be calculated to see whether or not they can successfully explain the properties of these interacting systems.

ACKNOWLEDGMENTS

We thank PPARC for the award of research grants that allowed this work to be completed. We thank the staff of the Dominion Astrophysical Observatory for their support over the observing nights.

REFERENCES

Böhm-Vitense, E., 1981, Ann. Rev. Astron. Astrophys., 19, p. 295
Budding, E., 1975, Astro. Space Sci., 36, 329
Chochol, D., 1977, IBVS 1237
Chochol, D., 1980, BAICz, 31, 321
Claret, A., Giménez, A., 1992, A&AS, 96, 255
Claret, A., Giménez, A., 1993, A&A, 277, 487
Conti, P.S., Alschuler, W.R., 1971, ApJ, 170, 325
Crawford, D.L., 1973, in IAU Symp. No. 54 'Problems of Calibration of Absolute Magnitudes and Temperature of Stars', B. Hauck, B.E. Westerlund (eds), Reidel (Dordrecht), p. 93
Crawford, D.L., 1975, PASP, 87, 481
Crawford, D.L., 1978, AJ, 83, 48
Crawford, D.L., 1994, PASP, 106, 397
Crawford, D.L., Barnes, J.V., Golson, J.C., 1971, AJ, 76, 1058
Crawford, D.L., Mandwewala, N., 1976, PASP, 88, 917
de Loore, C., Vanbevern, D., 1994a, A&A, 292, 463
de Loore, C., Vanbeveren, D., 1994b, A&AS, 105, 21
Drechsel, H., Haas, S., Lorenz, R., Mayer, P., 1994, A&A, 284, 853
Garmany, C.D., Stencel, R.E., 1992, A&AS, 94, 211
Harries, T.J., Hilditch, R.W., Hill, G., 1997, MNRAS, 285, 277
Harries, T.J., Hilditch, R.W., 1997, in 'BMW II title' ed. Howarth I.D., ASP Conf Series (in press)
Hauck, B., Mermilliod, M., 1980, A&AS, 40, 1
Hilditch, R.W., 1974, MNRAS, 169, 323
Hilditch, R.W., Hill, G., 1975, Mem. RAS, 79, 101
Hilditch, R.W., Harries, T.J., Bell, S.A., 1996, A&A, 314, 165
Hill, G., 1979, PDAO, 15, 297
Hill, G., 1982, PDAO, 16, 59
Hill, G., 1986, Unpublished DAO manual
Hill, G., Hilditch, R.W., Younger, F., Fisher, W.A., 1975, Mem. RAS, 79, 131
Hill, G., Hilditch, R.W., Pfannenschmid, F.L., 1976, PDAO, 15, 1

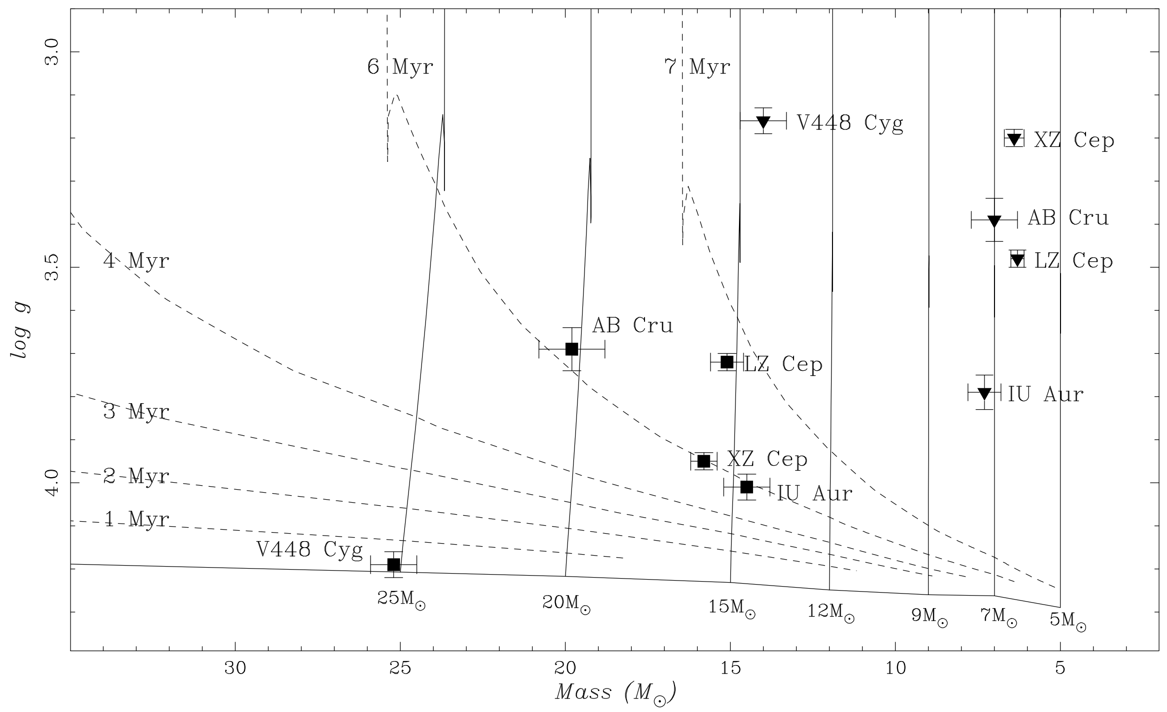

Figure 9. Primaries (filled squares) and secondaries (filled triangles) of semi-detached O+O binaries plotted in the mass–log g plane. The solid lines are the single star evolutionary tracks of Schaller et al. (1992), while the dashed lines represent isochrones for the same models.

Hill, G., Rucinski, S.M., 1993, in 'Light Curve Modeling of Eclipsing Binary Stars', ed. E.F. Milone, Springer-Verlag (New York), p. 135

Hill, G., Hilditch, R.W., Aikman, G.C.L., Khalesseh, B., 1994, A&A, 282, 455

Howarth, I.D., Stickland, D.J., Prinja, R.K., Koch, R.H., Pfeiffer, R.J., 1991, Obs, 111, 167

Howarth, I.D., Siebert, K.W., Hussain, G.A.J., Prinja, R.K., 1997, MNRAS, 284, 265

Hubeny, I., 1997, in 'Boulder-Munich II: Properties of Hot, Luminous Stars' ed. Howarth I.D., ASP Conf Series (in press)

Humphreys, R.M., 1978, ApJS, 38, 309

Liu, X., Leung, K.C., Tan, H., 1988, Chin. Astron., 12, 298

Lorenz, R., Mayer, P., Drechsel, H., 1994, A&A, 291, 185

Mammano, A., Margoni,R., Stagni, R., 1977, A&A, 59, 9

Mason, B.D., et al., 1997, AJ, (submitted)

Mayer, P., Drechsel, H., 1987, A&A, 183, 61

Mayer, P., Wolf, M., Termko, J., Niarchos, P.G., 1991, Bull. Astron. Inst. Czech., 42, 225

Mayer, P., Lorenz, R., Chocol, D., Irsmambetova, T.R., 1994, A&A, 288, L13

Ohmori, S., 1989, IBVS 3333

Petrie, R.M., 1962, PDAO, 12, 111

Schaller, G., Schaerer, D., Meynet, G., Maeder, A., 1992, A&AS, 96, 269

Vanbeveren, D., De Loore, C., 1994, A&A, 290, 129